Assessing different approaches to *ab initio* calculations of spin wave stiffness

O. Šipr ⓘ,[1,2,*] S. Mankovsky,[3] and H. Ebert[3]

[1]*FZU–Institute of Physics of the Czech Academy of Sciences, Cukrovarnická 10, CZ-162 53 Prague, Czech Republic*
[2]*New Technologies Research Centre, University of West Bohemia, Pilsen, Czech Republic*
[3]*Universität München, Department Chemie, Butenandtstr. 5-13, D-81377 München, Germany*

Ab initio calculations of the spin-wave stiffness constant D for elemental Fe and Ni performed by different groups in the past have led to values with a considerable spread of 50–100%. We present results for the stiffness constant D of Fe, Ni, and permalloy $Fe_{0.19}Ni_{0.81}$ obtained by three different approaches: (i) by finding the quadratic term coefficient of the power expansion of the spin-wave energy dispersion, (ii) by a damped real-space summation of weighted exchange coupling constants, and (iii) by integrating the appropriate expression in reciprocal space. All approaches are implemented by means of the same Korringa-Kohn-Rostoker (KKR) Green's function formalism. We demonstrate that if properly converged, all procedures yield comparable values, with uncertainties of 5–10% remaining. By a careful analysis of the influence of various technical parameters, we estimate the margin of errors for the stiffness constants evaluated by different approaches and suggest procedures to minimize the risk of getting incorrect results.

I. INTRODUCTION

Investigations of magnetic properties of materials at the phenomenological level based on a model spin Hamiltonian may be formulated either in a continuous field (micromagnetic) representation or in an atomistic representation. In the first case, the energy functional (neglecting relativistic effects) is given by [1]

$$E[\boldsymbol{m}] = \int_V d^3\boldsymbol{r} \, A_{\text{ex}} \sum_{c=x,y,z} \left(\frac{\partial \boldsymbol{m}}{\partial c} \right)^2, \quad (1)$$

where $\boldsymbol{m}(\boldsymbol{r})$ is the magnetization field and A_{ex} is the exchange stiffness constant. In the atomistic representation, the energy is given by the Heisenberg Hamiltonian,

$$H = -\sum_{ij} J_{ij} \, \hat{\boldsymbol{e}}_i \cdot \hat{\boldsymbol{e}}_j, \quad (2)$$

where $\hat{\boldsymbol{e}}_i$ and $\hat{\boldsymbol{e}}_j$ are unit vectors specifying the orientation of the magnetic moments for the atoms i and j, with the exchange coupling characterized by the exchange parameter J_{ij}. Both approaches give access to the energy of spin-wave excitations $\epsilon(\boldsymbol{q})$, which can be written in the long wave limit as [2]

$$\epsilon(\boldsymbol{q}) = D \, |\boldsymbol{q}|^2 + \dots, \quad (3)$$

where $\boldsymbol{q}$ is the corresponding wave vector and D is the spin-wave stiffness constant. The quantity is directly connected to the exchange stiffness A_{ex} via the relation [1]

$$A_{\text{ex}} = \frac{D M_s}{2g\mu_B}, \quad (4)$$

where M_s is the saturation magnetization, g is the Landé factor ($g \approx 2$ for metals) and μ_B is the Bohr magneton. This relation provides a link to the experiment: The model parameter A_{ex} entering Eq. (1) can be obtained from the spin-wave stiffness constant D, which can be determined experimentally. On the other hand, comparing the spin-wave stiffness calculated from first principles with experimental data allows us to assess the reliability of models and approximations used in the calculations.

As the spin-wave stiffness constant D characterizes the energy of spin-wave excitations in the long-wave limit, it can be obtained on the basis of spin spiral calculations within the adiabatic approximation. In this case, the energy $\epsilon(\boldsymbol{q})$ calculated from first principles for a spin spiral characterized by a wave vector $\boldsymbol{q}$ should be approximated around $\boldsymbol{q} = 0$ by a suitable polynomial and the stiffness constant D is just the expansion coefficient of the quadratic term.

A similar scheme can also be applied to evaluate D by using the spin-wave energy dispersion represented in terms of real-space interatomic exchange coupling parameters, obtained on the basis of the magnetic force theorem. In this case, by expressing the spin spiral energy in a power series of $\boldsymbol{q}$, one arrives at the expression [3–5]

$$D = \sum_j \frac{2\mu_B}{3\mu_j} J_{0j} R_{0j}^2, \quad (5)$$

where μ_j is the magnetic moment of atom j and R_{0j} is the corresponding interatomic distance.

Both approaches, i.e., the one based on fitting calculated spin spiral energies by a polynomial and the one based on evaluating the real-space sum Eq. (5), were employed for *ab initio* calculations of the spin-wave stiffness constant D in the past. However, despite the conceptual simplicity of both procedures, values of D obtained by different groups for the

*sipr@fzu.cz; http://crysa.fzu.cz/ondra

TABLE I. Previous theoretical results for the spin-wave stiffness D (in meV Å^2) of elemental Fe and Ni and of Fe$_{1-x}$Ni$_x$ alloy (its composition was Fe$_{0.25}$Ni$_{0.75}$ [6] and Fe$_{0.19}$Ni$_{0.81}$ [7]). Each study is identified by a reference and the publication year. The method how D was evaluated is indicated in the last column: $\epsilon(\boldsymbol{q})$ stands for fitting the spin-wave dispersion Eq. (3) whereas J_{ij} denotes a weighted sum of the coupling constants Eq. (5).

Work		Fe	Ni	Fe$_{1-x}$Ni$_x$	Method
[8]	(1996)	214	527		J_{ij}
[9]	(1997)	247	739		J_{ij}
[10]	(1999)	135	180		$\epsilon(\boldsymbol{q})$
[11]	(1999)	280	740		$\epsilon(\boldsymbol{q})$
[2]	(2000)	355	790		$\epsilon(\boldsymbol{q})$
[5]	(2001)	250	756		J_{ij}
[12]	(2003)	200			$\epsilon(\boldsymbol{q})$
[6]	(2008)			515	J_{ij}
[13]	(2005)	322	541		$\epsilon(\boldsymbol{q})$
[7]	(2017)	320	707	620	J_{ij}

same systems exhibit a considerable spread. To illustrate this, we present in Table I several values for the stiffness constant D for elemental Fe and Ni and permalloy Fe$_{0.19}$Ni$_{0.81}$ (Py) obtained by previous theoretical studies. Another comparison can be found, e.g., in Table 10 of Vaz *et al.* [1]. One can see from Table I that the deviations may easily reach 50%. Such big discrepancies are extraordinarily high when compared, for example, with the situation for the exchange coupling parameters J_{ij}—even when considering that the studies employ different methods of electronic structure calculations relying on different approximations. The discrepancies also appear between studies which use the same method to evaluate the stiffness constant D: It is not that results based on one method would cluster around one value and results based on the other method around another value. As none of the previous studies presented results obtained by both methods—one always focused solely either on Eq. (3) or on Eq. (5)—it is difficult to assess properly the accuracy and reliability of the procedures involved.

Yet another way to determine the spin-wave stiffness as the second derivative of the spin-wave energy with respect to the wave vector $\boldsymbol{q}$ relies on evaluating the corresponding derivatives of the exchange parameters $J(\boldsymbol{q})$. This in turn leads to an expression for the stiffness constant D formulated in reciprocal space, as presented by Liechtenstein *et al.* [3,4]. So far, no results on spin-wave stiffness based on this third approach have been reported in the literature. Only recently, a relativistic extension of the reciprocal-space expression for D was presented by Mankovsky *et al.* [14] and applied for studying Fe-Ni alloys.

The stiffness constant D is an important characteristic quantity as it determines—together with the magnetic anisotropy—the domain structure of magnetic materials. In addition, it determines the magnetization dynamics. Therefore, there is an urgent need for a detailed comparison of the various computational approaches to evaluate D so that reliable values can be obtained.

The aim of this paper is therefore to calculate the spin-wave stiffness constant D of Fe, Ni, and Py by analyzing the

long-wave limit of the spin-wave dispersion relation Eq. (3), by evaluating the weighted sum of coupling constants Eq. (5), and by a direct evaluation of D in reciprocal space [14]. All three approaches are implemented by use of the same electronic structure method, namely, the Korringa-Kohn-Rostoker (KKR) Green's function formalism, meaning that the results are directly comparable. A careful analysis of the influence of various technical parameters makes it possible to estimate the margin of errors for the stiffness constants evaluated by the different approaches and to decide whether there is a significant difference between them or not. By illustrating how various factors affect the outcome, we offer a guidance how the procedures ought to be performed to minimize the risks of wrong results.

II. COMPUTATIONAL SCHEME

Evaluation of the spin-wave stiffness constant D is done on the basis of a calculation of the underlying electronic structure of the system. For this, we employed the *ab initio* spin-polarized multiple scattering or KKR Green's function formalism [15] as implemented in the SPRKKR code [16]. The calculations were performed in a scalar-relativistic mode, relying on the generalized gradient approximation to the spin-density functional theory, using the Perdew, Burke, and Ernzerhof functional. For the multipole expansion of the Green's function, an angular momentum cutoff $\ell_{\max} = 3$ was used. The potentials were subject to the atomic sphere approximation (ASA). When dealing with Py, the substitutional disorder was accounted for within the coherent potential approximation. The energy integrals were evaluated by contour integration on a semicircular path within the complex energy plane, using a Gaussian mesh of 32 points. The $\boldsymbol{k}$-space integration was carried out via sampling on a regular mesh, making use of the symmetry. The number of $\boldsymbol{k}$ points in the mesh is an important technical parameter and will be considered in Sec. III in more detail; here we just note that unless specified otherwise, we used 89^3 points in the full Brillouin zone (BZ) for bcc Fe, 112^3 points for fcc Ni, and 75^3 points for fcc Py. The equilibrium lattice constant a_0 was determined by minimizing the total energy for each system. This gives us $a_0 = 2.830$ Å for Fe, 3.506 Å for Ni, and 3.523 Å for Py.

To evaluate the stiffness constant D by means of finding the expansion coefficient as in Eq. (3), the spin-wave energy dispersion relation $\epsilon(\boldsymbol{q})$ has to be obtained. We achieved this by evaluating the change of the total energy per unit cell $E(\boldsymbol{q}, \theta) - E(0, \theta)$ due to a spin spiral characterized by magnetic moment

$$\mu_{\text{spin}} [\cos(\boldsymbol{q}\boldsymbol{R}) \sin \theta, \sin(\boldsymbol{q}\boldsymbol{R}) \sin \theta, \cos \theta], \tag{6}$$

where $\boldsymbol{R}$ is the Bravais lattice vector, $\boldsymbol{q}$ is the spin spiral wave vector, θ is the spiral cone angle, and μ_{spin} is the magnitude of the magnetic moment per site. The magnon energy $\epsilon(\boldsymbol{q})$ is given by [2]

$$\epsilon(\boldsymbol{q}) = \lim_{\theta \to 0} \frac{4\mu_B}{\mu_{\text{spin}}} \frac{E(\boldsymbol{q}, \theta) - E(0, \theta)}{\sin^2 \theta}. \tag{7}$$

The change of the energy $E(\boldsymbol{q}, \theta) - E(0, \theta)$ due to the spin spiral Eq. (6) can be obtained either by employing self-consistent calculations for each of the wave vectors $\boldsymbol{q}$ or by

relying on the force theorem, meaning that the same potential (obtained for the ferromagnetic state) for all wave vectors $\boldsymbol{q}$ is used. The electronic structure for spiral magnetic order was calculated as described by Mankovsky *et al.* [17]. Our calculations are scalar-relativistic, therefore, the results do not depend on the angle between the axis of the spin rotation cone and the spin-wave propagation direction. The details how the behavior of $\epsilon(\boldsymbol{q})$ for $\boldsymbol{q} \to 0$ was analyzed are described in detail in Sec. III A.

When resorting to the second option, namely, an evaluation of the stiffness constant D in real space by relying on Eq. (5), one has to deal with the fact that the sum over the atoms $\sum_j$ in Eq. (5) does not converge for metals (due to the long-range character of the exchange coupling) [5]. Hence, an additional damping factor has been introduced which enables evaluation of Eq. (5) by extrapolating the partial results to zero damping [5]. In particular, we evaluated the stiffness constant D as [5,18,19]

$$D = \lim_{\eta \to 0} D(\eta), \tag{8}$$

$$D(\eta) = \sum_{\alpha} c_{\alpha} D_{\alpha}(\eta), \tag{9}$$

$$D_{\alpha}(\eta) = \sum_{j} \sum_{\beta} c_{\beta} \frac{2\mu_B}{3\sqrt{|\mu_{\alpha}||\mu_{\beta}|}} J_{0j}^{(\alpha\beta)} R_{0j}^2 \, e^{-\eta \frac{R_{0j}}{R_{01}}}, \tag{10}$$

where j labels the lattice sites, c_{α} and μ_{α} are the concentration and the magnetic moment of atoms of type α, $J_{0j}^{(\alpha\beta)}$ is the pairwise exchange coupling constant if an atom of type α is located at the lattice origin and an atom of type β is located at the lattice site j, R_{0j} is the distance of the site j from the lattice origin, η is the damping parameter and R_{01} is the nearest-neighbor interatomic distance [5,18–20]. Note that we have one atomic type for Fe and Ni whereas two atomic types for Py. The exchange coupling constants $J_{0j}^{(\alpha\beta)}$ were evaluated from the electronic structure using the prescription of Liechtenstein *et al.* [4]. Taking the limit $\lim_{\eta \to 0} D(\eta)$ in Eq. (8) is a delicate issue and we devote to it most of Sec. III B.

Performing the sum over atomic sites in Eq. (5) or Eqs. (9)–(10) can be by-passed by evaluating the stiffness constant D via a reciprocal-space integration [3,4]. A recently reported relativistic generalization of this approach [14] leads to the expression:

$$
\begin{aligned}
D_{\alpha\beta} = \frac{1}{\pi \mu_{\text{spin}}} \text{ImTr} \int^{E_F} dE \, \frac{1}{\Omega_{\text{BZ}}} \int_{\text{BZ}} d^3 k \\
\times \left[\underline{T}_x \frac{\partial \underline{\tau}(\boldsymbol{k}, E)}{\partial k_{\alpha}} \underline{T}_x \frac{\partial \underline{\tau}(\boldsymbol{k}, E)}{\partial k_{\beta}} \right. \\
\left. + \underline{T}_y \frac{\partial \underline{\tau}(\boldsymbol{k}, E)}{\partial k_{\alpha}} \underline{T}_y \frac{\partial \underline{\tau}(\boldsymbol{k}, E)}{\partial k_{\beta}} \right].
\end{aligned}
\tag{11}
$$

The matrix $\underline{\tau}$ is the Fourier transform of the scattering path operator and the matrices $\underline{T}_x$, $\underline{T}_y$ represent the change of the potential upon rotating the spin,

$$T_{x,\Lambda_1\Lambda_2} = \int d^3 r \, Z_{\Lambda_1}^{\times}(\boldsymbol{r}, E) \, \beta \sigma_x \, Z_{\Lambda_2}(\boldsymbol{r}, E), \tag{12}$$

$$T_{y,\Lambda_1\Lambda_2} = \int d^3 r \, Z_{\Lambda_1}^{\times}(\boldsymbol{r}, E) \, \beta \sigma_y \, Z_{\Lambda_2}(\boldsymbol{r}, E), \tag{13}$$

where $Z_{\Lambda}(\boldsymbol{r}, E)$ stands for the regular solution of a single-site Dirac equation, and subscripts α, β denote cartesian components. We deal with cubic lattices, so the stiffness constant D is isotropic, $D_{xx} = D_{yy} = D_{zz} = D$. For more details, see the original paper [14]. The advantage of using Eq. (11) is that there is no need for polynomial fitting as when employing Eqs. (3) and (7) or for extrapolation as when employing Eq. (8). On the other hand, when proceeding along Eq. (11), one has to evaluate the derivative $(\partial \tau / \partial k)$ which is a numerically demanding task.

In this work we evaluated the integrand in Eq. (11) using the same scalar-relativistic potential as when obtaining the stiffness constant D via Eqs. (3) and (7) or via Eqs. (8)–(10). Moreover, we suppress the spin-orbit coupling (SOC) by employing an approximate two-component scheme [21], similarly as when investigating the influence of SOC on electronic-structure-related properties in the past [22,23]. The results we obtain by means of Eq. (11) are thus directly comparable to scalar-relativistic results obtained by means of the other two approaches. The $\boldsymbol{k}$-mesh used for this type of calculations contained 135^3 points for Fe and Py and 144^3 points for Ni.

Let us note finally that even though we employ a particular electronic structure calculation method (KKR Green's function formalism), the issues we deal with are not specific to it and will have to be cared upon no matter which calculational method is used.

III. RESULTS

A. Fitting spin-wave energy dispersion

First we consider various aspects when obtaining the spin-wave stiffness constant D as the coefficient of the quadratic term of the power expansion for the spin-wave energy dispersion relation Eq. (3). An obvious technical parameter against which the convergence should be checked is the density of the mesh used to evaluate the integrals in $\boldsymbol{k}$-space. We verified that for the grids used in this section, namely, 165^3 points in the full BZ for Fe, to 149^3 points for Ni, and to 133^3 points for Py, the values of D are converged within ± 0.2 meV Å^2. This means that for the purpose of the convergency tests outlined in this section, the values of D can be considered as practically accurate in this regard.

The magnon energy $\epsilon(\boldsymbol{q})$ is represented in terms of the spin-spiral energy Eq. (7) in the limit $\theta \to 0$. For this one should calculate the electronic structure for spin spirals with the cone angle θ as small as possible. However, if the angle θ approaches zero, so does the energy difference $E(\boldsymbol{q}, \theta) - E(0, \theta)$, and evaluating the ratio $[E(\boldsymbol{q}, \theta) - E(0, \theta)]/\sin^2 \theta$ becomes numerically unstable. Therefore, we start by looking closely on the sensitivity of $[E(\boldsymbol{q}, \theta) - E(0, \theta)]/\sin^2 \theta$ to the value of θ.

To get an overview, we plot the ratio

$$\frac{E(\boldsymbol{q}, \theta) - E(0, \theta)}{\sin^2 \theta} \tag{14}$$

as a function of the wave vector $\boldsymbol{q}$ for several values of the cone angle θ. This is done in the upper panels of Figs. 1 and 2 for Fe and Ni, respectively. The wave vector $\boldsymbol{q}$ is oriented along the [001] direction. The corresponding spin spiral
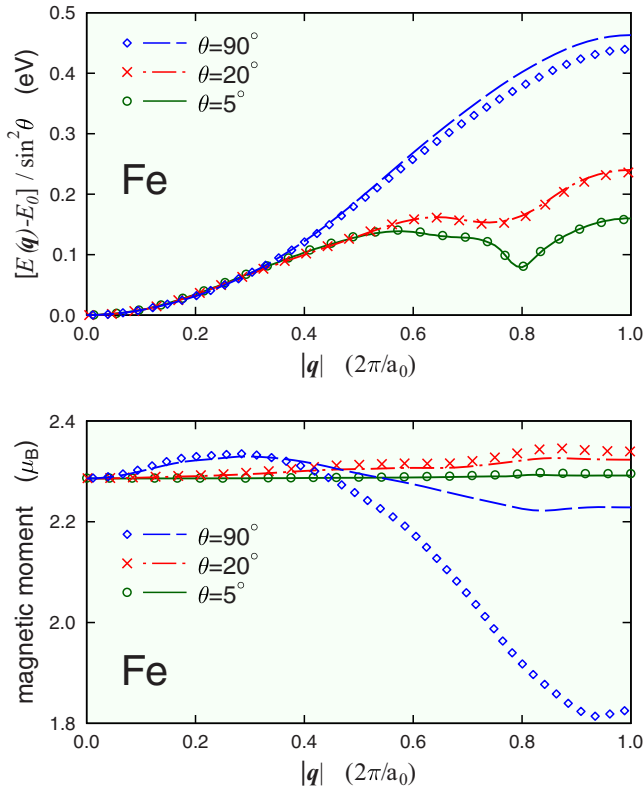
FIG. 1. Magnetic moment per atom (lower panel) and energy dispersion $[E(\boldsymbol{q}) - E_0]/\sin^2\theta$ (upper panel) for spin spiral waves propagated along the [001] direction in Fe, obtained by means of self-consistent calculations (markers) and by means of magnetic force theorem (lines). The spiral cone angle θ is specified in the legend.

FIG. 2. As Fig. 1 but for Ni. Note that the energy dispersion curves for $\theta = 5°$ and $20°$ almost coincide.

energies were calculated by means of self-consistent calculations (SCF), i.e., with the potential recalculated for each $\boldsymbol{q}$ vector (shown via markers), as well as using the magnetic force theorem (MFT), with the potential taken always the same as for $\boldsymbol{q} = 0$ (shown via lines). Additionally, we present data on magnetic moments in the lower panels of Figs. 1–2, to provide a more complete picture. Interestingly, the magnetic moment is more sensitive to whether the calculation is done self-consistently or not than the energy is — especially if $|\boldsymbol{q}|$ gets large. The sudden decrease of μ_{spin} of Ni at about $0.5(2\pi/a_0)$ clearly seen for $\theta = 90°$ (Fig. 2) corresponds to the well-known collapse of the magnetic moment of Ni in case of anti-ferromagnetic order [9,24].

Based on the curves in Figs. 1 and 2, it appears that for $|\boldsymbol{q}|$ less than about $0.2(2\pi/a_0)$, the ratio Eq. (14) depends only little on θ and that the differences between SCF and MFT calculations are small. To get more quantitative information on the dependence of the expression in Eq. (14) on the cone angle θ, we summarize in Tables II–IV the values of D obtained by fitting a bi-quadratic function

$$f_4(q, \theta) = a_2(\theta)q^2 + a_4(\theta)q^4, \tag{15}$$

to the energy

$$\epsilon(\boldsymbol{q}, \theta) = \frac{4\mu_B}{\mu_{\text{spin}}} \frac{E(\boldsymbol{q}, \theta) - E(0, \theta)}{\sin^2\theta} \tag{16}$$
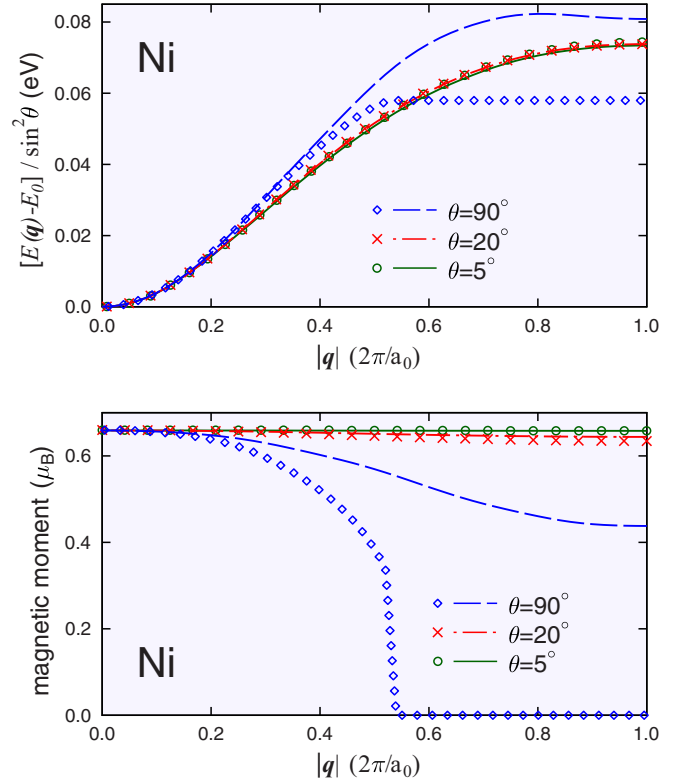
in the interval $|\boldsymbol{q}| \in [0, 0.1(2\pi/a_0)]$, for different values of the cone angle θ. The stiffness constant D is obtained as the expansion coefficient of the quadratic term,

$$D = a_2(\theta).$$

The necessary $\boldsymbol{k}$-space integrals were evaluated using a regular mesh corresponding to 165^3 points in the full BZ for Fe, to 149^3 points for Ni, and to 133^3 points for Py. The results based on SCF and MFT calculations are shown separately. The $\boldsymbol{q}$-vector was varied along the [001] direction, the fit was obtained for values of $|\boldsymbol{q}|$ from zero to $0.1(2\pi/a_0)$. Data for $\theta < 20°$ are not included in Tables II–IV because for small values of θ the stability of the fit gets worse due to very small differences $E(\boldsymbol{q}, \theta) - E(0, \theta)$ and the results are not reliable.

One can infer from Tables II–IV that going to very low values of θ is not needed for spin-wave stiffness calculations.

TABLE II. Spin wave stiffness constant D of Fe evaluated by fitting the energy dispersion Eq. (16) for $\boldsymbol{q} \to 0$ by a biquadratic polynomial Eq. (15), for spiral cones angles $\theta = 20°$, $45°$, and $90°$. The energies were obtained either from self-consistent calculations (SCF) or by employing the magnetic force theorem (MFT).

θ (deg)	SCF D (meV Å^2)	MFT D (meV Å^2)
20	302.4	292.8
45	301.1	292.3
90	301.7	294.0

TABLE III. Same as Table II but for Ni.

θ (deg)	SCF D (meV Å^2)	MFT D (meV Å^2)
20	752.4	747.9
45	753.4	746.9
90	755.7	745.9

The energy $\epsilon(\boldsymbol{q}, \theta)$ is practically independent on the cone angle θ. Consequently, all the spin spiral calculations are done for $\theta = 20°$ in the rest of the paper, because this value appears to be a good representation of $\theta \to 0$ for the purpose of evaluating Eq. (7) and still is large enough to lead to numerically stable results.

To obtain correct and unambiguous results on D from spin spirals energies, as outlined by Eqs. (3) and (7), it is necessary to assess critically the fitting procedure which provides the D coefficient. To find the power expansion of the energy Eq. (7), the function $\epsilon(\boldsymbol{q})$ is fitted by a polynomial via a least-squares method, within a certain interval of $\boldsymbol{q}$. Therefore one has to check how the expansion coefficient D is affected by the degree of the polynomial which is fitted to $\epsilon(\boldsymbol{q})$ and also by the size of the interval within which this fit is determined.

Concerning the choice of the interval for the fit, there is the natural requirement that the interval is not very large, because a fit within a small interval emphasizes the behavior of $\epsilon(\boldsymbol{q})$ at the origin and that is what we aim at. However, for small q, there are technical problems with the numerical accuracy of the difference $E(\boldsymbol{q}, \theta) - E(0, \theta)$. Namely, if the number of $\boldsymbol{k}$-points increases, the energy dispersion curves $E(\boldsymbol{q}, \theta)$ approach each other not uniformly but in a quasi-oscillatory way. This is illustrated in Fig. 3 where the energy dispersion $[E(\boldsymbol{q}) - E_0]/\sin^2 \theta$ for spin spiral waves in Fe obtained using different $\boldsymbol{k}$-meshes is displayed very close to the origin $|\boldsymbol{q}| = 0$. One can see that fine details of the energy dispersion still vary even for quite dense meshes. If the $\boldsymbol{k}$-mesh density is not high enough, the behavior of the $\epsilon(\boldsymbol{q})$ function may significantly deviate from the expected form. E.g., for the mesh with 106^3 points, there is actually a local *maximum* at $q = 0$; it is shallow and can be seen only if the step in q is sufficiently small but it clearly hinders finding the correct power expansion coefficients. If one wants to by-pass the numerical problems with determining $E(\boldsymbol{q}, \theta) - E(0, \theta)$ for small q by performing the fit within a large interval, one has to include more terms in the fitting polynomial, because as one moves away from $q = 0$, higher order terms get more important. A proper balance between the size of the interval in which the fit to $\epsilon(\boldsymbol{q})$ is performed and the order of the fitting polynomial thus has to be achieved.

TABLE IV. Same as Table II but for Py.

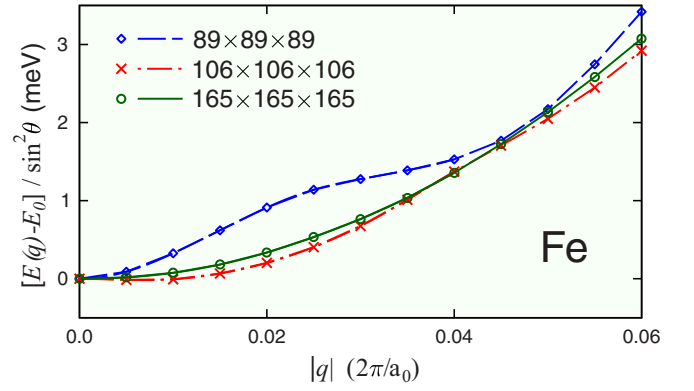| θ (deg)	SCF D (meV Å^2)	MFT D (meV Å^2)
20	519.7	520.6
45	521.6	522.9
90	521.2	522.2

FIG. 3. The energy dispersion $[E(\boldsymbol{q}) - E_0]/\sin^2 \theta$ for spin spiral waves in Fe obtained when the $\boldsymbol{k}$-space integrals were evaluated using a regular mesh corresponding to 89^3 points, 106^3 points, and 165^3 points in the full BZ. The $\boldsymbol{q}$-vector was varied along the [001] direction and the cone angle is $\theta = 20°$. The energies were calculated employing self-consistent potentials.

Tables V–VII summarize the stiffness constant D for Fe, Ni, and Py evaluated by fitting the energy dispersion Eq. (7) to polynomials of different degrees, within intervals of different sizes. We consider polynomials of even powers only (because of the symmetry), they can be symbolically written as

$$f_{2n}(\boldsymbol{q}) = \sum_{i=1}^{n} a_{2i} q^{2i}. \tag{17}$$

The spin-wave stiffness constant D corresponds to the quadratic term,

$$D = a_2. \tag{18}$$

The highest degree of a polynomial employed within this study is twelve. The spiral cone angle was set to $\theta = 20°$, energies were obtained by means of self-consistent calculations, and the $\boldsymbol{k}$-space integration was carried out on a mesh of 165^3 points in the full BZ for Fe, 149^3 points for Ni, and 133^3 points for Py.

Inspecting Tables V–VII gives an idea about the stability of the procedure. Fitting $\epsilon(\boldsymbol{q})$ within the smallest interval $[0, 0.05]$ (in units of $2\pi/a_0$) is clearly unstable, due to the problems with the $\boldsymbol{k}$-mesh convergence (see also Fig. 3). When fitting within larger intervals, one should employ

TABLE V. Spin wave stiffness constant D (in meV Å^2) of Fe evaluated by fitting the energy dispersion Eq. (7) by polynomials Eq. (17) of degrees $2n = 2, 4, 6, 8,$ and 12, within intervals of different sizes.

polyn. degree	interval for fitting (in units of $2\pi/a_0$)			
	$[0, 0.05]$	$[0, 0.10]$	$[0, 0.15]$	$[0, 0.20]$
4	301.0	302.6	302.5	316.8
6	303.6	302.6	298.6	298.1
8	298.6	301.6	305.0	294.3
10	276.2	301.6	304.8	302.8
12	251.6	302.1	300.6	302.8

TABLE VI. As Table V but for Ni.

polyn. degree	interval for fitting (in units of $2\pi/a_0$)			
	[0, 0.05]	[0, 0.10]	[0, 0.15]	[0, 0.20]
4	746.3	751.9	761.7	768.8
6	774.1	747.5	749.1	760.2
8	648.9	747.8	749.0	750.3
10	463.9	747.2	747.4	747.6
12	353.6	747.1	748.8	745.1

polynomials of at least sixth degree. For the largest interval [0, 0.20], the results sometimes depend on the choice of the polynomial even up to the twelfth degree (see Table VI), suggesting that more complicated trends which cannot be described by a simple polynomial may be present (see the upper panels of Figs. 1 and 2 for an overall picture). As a whole, however, for each of the systems one can find a "region of stability" at the bottom right corner of the respective table, where the values do not significantly depend on the size of the fitting interval or on the degree of the fitting polynomial (within the accuracy of ± 0.2 meV Å^2 determined by the $\boldsymbol{k}$-mesh convergence). The numbers in this region do not depend on the fine details of how the coefficient at the quadratic term has been determined, therefore, they can be considered as the correct artefact-free values of the stiffness constant D. The spread of the values within this region can be used to estimate the error of D if it is determined by fitting the spin-wave energy dispersion.

B. Weighted sum of J_{ij} constants

In this section, we inspect problems that may be encountered when evaluating the stiffness constant D via a weighted sum of the coupling constants J_{ij}, as in Eqs. (8)–(10). Basic understanding can be gained by looking on the dependence of D on the maximum distance $R_{\max}$ up to which the individual terms in Eq. (10) are evaluated. This is presented in Fig. 4 for Ni and Py, for several values of the damping parameter η. One can see that the quasi-oscillations of $D(R_{\max})$ extend to quite large distances and that the limiting value $\lim_{R_{\max}\to\infty} D(R_{\max})$ depends on the damping parameter η.

The stiffness constant D is finally determined via $D = \lim_{\eta\to 0} D(\eta)$. The limit has to be found by extrapolating $D(\eta)$ down to $\eta = 0$. Therefore, one should evaluate $D(\eta)$ for as small η as possible. Fig. 4 demonstrates that to evaluate $D(\eta)$ for small η, one has to extend the sum in Eq. (10) up to

TABLE VII. As Table V but for Py.

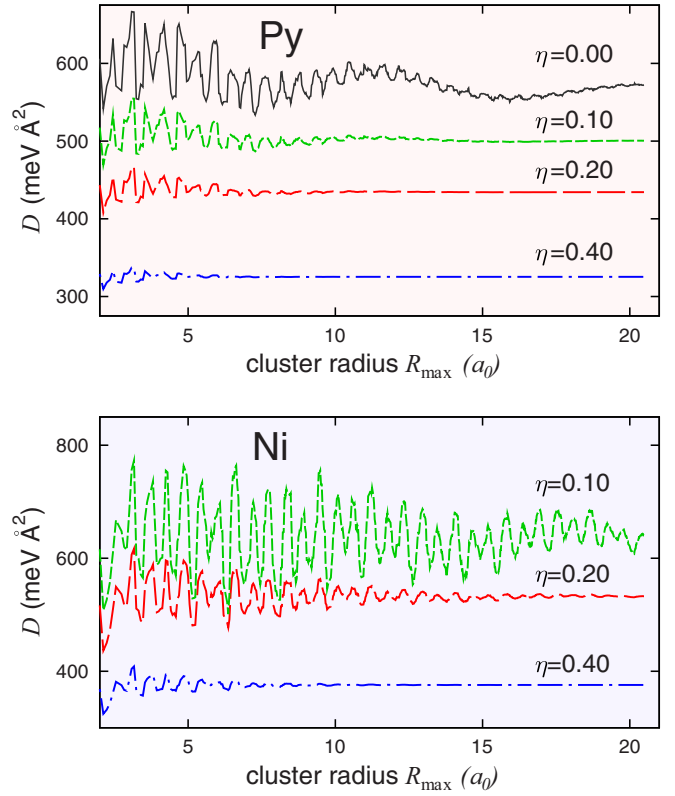| polyn. degree	interval for fitting (in units of $2\pi/a_0$)			
	[0, 0.05]	[0, 0.10]	[0, 0.15]	[0, 0.20]
4	534.4	519.8	525.5	528.4
6	505.2	518.9	521.0	524.5
8	342.9	518.0	521.6	521.4
10	205.7	499.0	521.5	520.6
12	170.6	535.4	521.2	520.9

FIG. 4. Dependence of the spin-wave stiffness constant D on the maximum distance $R_{\max}$ up to which the terms in Eq. (10) are included, for different damping parameters η. Lower panel shows data for for Ni obtained using the mesh of 112^3 points in the full BZ, upper panel shows data for Py obtained using the mesh of 75^3 points in the full BZ. The distance $R_{\max}$ is in units of the lattice constant a_0.

large $R_{\max}$. Evaluating the exchange coupling constants J_{ij} for large interatomic distances requires a high density of the mesh used for integration in $\boldsymbol{k}$ space [5]. To illustrate this, we present in Fig. 5 the dependence of the constant D of Ni on the cut-off distance $R_{\max}$, for several $\boldsymbol{k}$-space grids. It can be seen immediately that going to larger $R_{\max}$ requires a denser
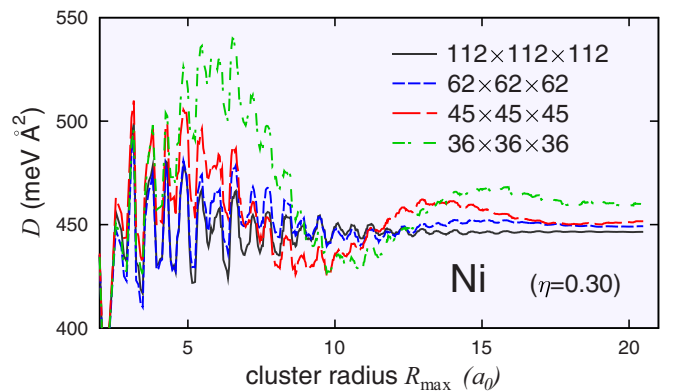

FIG. 5. Dependence of the stiffness constant D for Ni on the maximum distance $R_{\max}$ up to which the terms in Eq. (10) are included, for different numbers of $\boldsymbol{k}$ points in the full BZ (shown in the legend). The data were obtained for damping parameter $\eta = 0.30$.
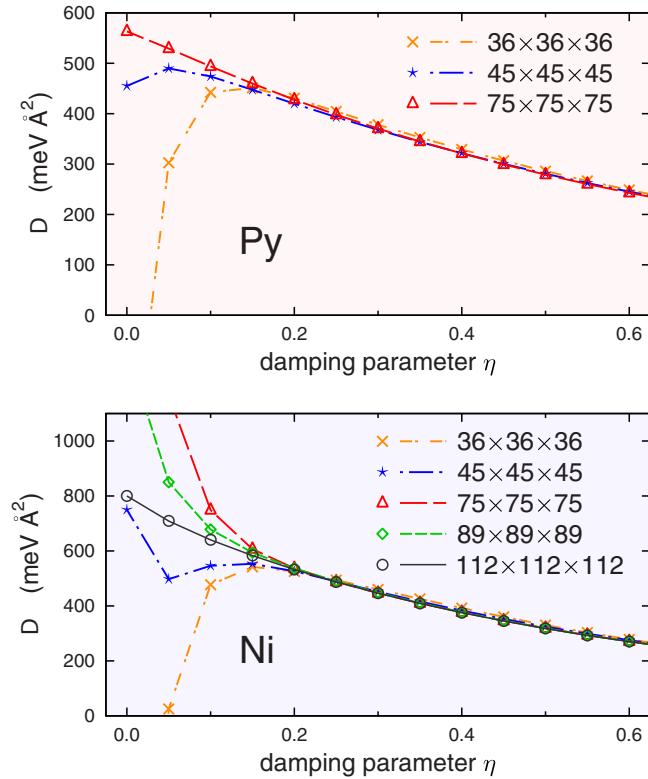
FIG. 6. Dependence of the spin-wave stiffness constant D for Ni (lower panel) and for Py (upper panel) on the damping parameter η. Data are shown for different $\boldsymbol{k}$-space grids. The maximum distance R_{max} up to which the individual terms in Eq. (10) were evaluated is $20.5a_0$.

$\boldsymbol{k}$-mesh, increasing dramatically the demand on conputational resources.

The conclusion is thus the following: if we want to evaluate the stiffness constant D via Eq. (5), we have to extrapolate $D(\eta)$ to $\eta = 0$, which requires obtaining $D(\eta)$ for small η's, which requires extending the sum in Eq. (10) to large R_{max} and that requires a high density for the $\boldsymbol{k}$-mesh. Graphically this is depicted in Fig. 6, where we show how the stiffness constant $D(\eta)$ of Ni and Py depends on the damping parameter η, for several choices of the $\boldsymbol{k}$-mesh. The summation in Eq. (10) covers interatomic distances up to $R_{max} = 20.5a_0$. It can be clearly seen that if the η parameter is relatively large, the values of $D(\eta)$ do not depend on the $\boldsymbol{k}$-mesh; the situation is numerically stable. However, for small η, the values of $D(\eta)$ depend strongly on the $\boldsymbol{k}$-mesh density. Data for $\eta < 0.2$ cannot be regarded as numerically stable.

The fact that the values of $D(\eta)$ obtained for low η are not reliable questions the accuracy with which the stiffness constant can be determined. The extrapolation of $D(\eta)$ to $\eta = 0$ is, obviously, a delicate procedure depending on several technical parameters. This is illustrated in Tables VIII–X where we show the stiffness constant D for Fe, Ni, and Py obtained by extrapolating $D(\eta)$ to $\eta = 0$ using different methods. In particular, the extrapolation was done using a polynomial of the second, third, or fifth degree in η, determined by least-squares fitting of $D(\eta)$ when η lies in the interval $[0.2,1]$, $[0.4,1]$, or $[0.6,1]$. The summation Eq. (10) includes all sites

TABLE VIII. Spin wave stiffness constant D of Fe evaluated by summing the $J_{0j}R_{0j}^2$ terms, Eqs. (8)–(10). The extrapolation of $D(\eta)$ to $\eta = 0$ has been done by fitting $D(\eta)$ by a polynomial, within specific intervals of η values. The interval within which the fit is done is specified in the first column, further columns contain values of D obtained by employing a fitting polynomial of the second, third, and fifth degree in η.

η interval	2nd degree D (meV Å^2)	3rd degree D (meV Å^2)	5th degree D (meV Å^2)
0.2–1.0	269.7	278.1	281.6
0.4–1.0	261.7	275.7	276.8
0.6–1.0	252.9	273.0	296.7

up to the distance $R_{max} = 20.5a_0$, which means about 70000 atoms (563 coordination shells) for bcc Fe and about 136000 atoms (773 coordination shells) for fcc Ni and Py. The $\boldsymbol{k}$-space integrals needed to evaluate the J_{ij} constants were carried out on a mesh of 89^3 points in the full BZ for Fe, 112^3 points for Ni, and 75^3 points for Py.

One can see from Tables VIII–X that the extrapolated values $D(\eta \to 0)$ significantly depend on the choice of the fitting interval. The most conclusive estimates of D are those obtained using a polynomial fitted to $D(\eta)$ within an interval which includes the smallest usable values for η, i.e., $\eta \in [0.2$–$1.0]$. Decreasing the lower boundary of the fitting interval even further is not desirable because the values of $D(\eta)$ may be numerically unstable for $\eta < 0.2$ (see Fig. 4). As concerns the degree of the polynomial used for the extrapolation: if the extrapolation is done via the second degree polynomial in η, the outcome significantly depends on the choice of the interpolating interval. This can hardly be considered as robust or stable. On the other hand, for the fifth-degree polynomial, this dependence is only mild. For the third degree polynomial, the situation is somewhere in between. We can thus conclude that estimating the stiffness constant D by fitting the $D(\eta)$ dependence by a fifth degree polynomial in η leads to trustworthy results.

A complementary picture can be obtained by inspecting Fig. 7, where we show the calculated values of $D(\eta)$ for Ni, together with three different polynomial fits of the $D(\eta)$ dependence. Note that if $\eta \leqslant 0.10$, the values of $D(\eta)$ contain significant numerical errors (see the bottom panel of Fig. 4) — we indicate this by errorbars. The polynomials of the second, third, and fifth degree in η were obtained by a least-squares fit for $\eta \in [0.4,1.0]$. One can see that the quadratic fit (green dash-dotted line) fails to reproduce $D(\eta)$ outside the fitting

TABLE IX. As Table VIII but for Ni.

η interval	2nd degree D (meV Å^2)	3rd degree D (meV Å^2)	5th degree D (meV Å^2)
0.2–1.0	708.3	754.6	768.1
0.4–1.0	663.2	736.7	769.1
0.6–1.0	618.2	712.9	785.5

TABLE X. As Table VIII but for Py.

η interval	2nd degree D (meV Å^2)	3rd degree D (meV Å^2)	5th degree D (meV Å^2)
0.2–1.0	539.4	560.6	563.1
0.4–1.0	518.5	555.1	565.4
0.6–1.0	495.9	546.1	567.6

range — it significantly deviates from the values marked by open circles in Fig. 7. The situation is better for the cubic fit. The best outcome is apparently achieved if the fit is done by a fifth-degree polynomial.

C. Direct evaluation of D in reciprocal space

The third way to calculate the spin-wave stiffness constant D is via integrating the relevant expression in reciprocal space, according to Eq. (11). As this is a direct evaluation, no analysis of the fitting or extrapolation procedure is needed. The values we obtained from Eq. (11) are given in the fourth column of Table XI.

IV. DISCUSSION

Our goal was to critically review different approaches to calculate the spin-wave stiffness constant D and to compare the results calculated for selected systems on the same footing. The approaches we investigated include (i) examining the long-wave-length behavior of the spin-wave energy dispersion [see Eqs. (3) and (7) and Sec. III A], (ii) evaluating a weighted sum of exchange coupling constants [Eqs. (8)–(10) and Sec. III B], and (iii) direct evaluation of Eq. (11) in reciprocal space. The results for Fe, Ni, and Py obtained by these methods are summarized in Table XI. The errors
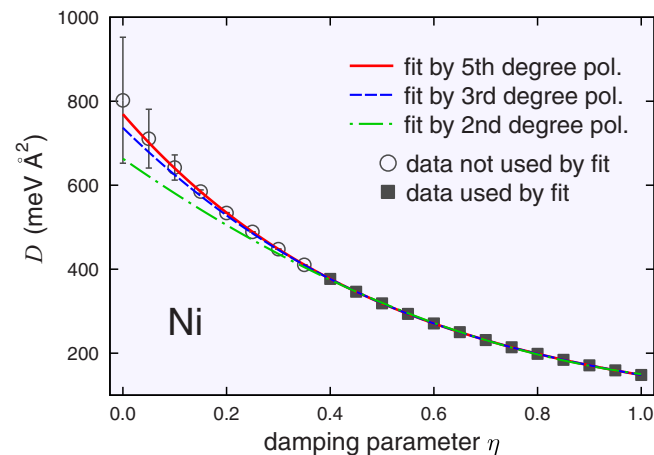

FIG. 7. Dependence of the spin-wave stiffness constant D for Ni on the damping parameter η, together with fits of $D(\eta)$ by polynomials of the second, third, and fifth degree in η (as indicated by the legend). To obtain the fitting polynomials, only data for $\eta \in [0.4, 1.0]$ were used. The $\boldsymbol{k}$-space integrals were evaluated using the grid of 112^3 points in the full BZ, the maximum distance $R_{\max}$ up to which the terms in Eq. (10) were included is $20.5a_0$.

TABLE XI. Overall estimates of the stiffness constant D for Fe, Ni, and Py based on fitting the spin-wave energy dispersion as in Eq. (3) (second column), by performing a weighted sum of J_{ij} constants as in Eq. (5) (third column), and by a direct integration of scattering matrices and operators in reciprocal space as in Eq. (11) (fourth column).

	From $\epsilon(\boldsymbol{q})$	From $\sum J_{0j} R_{0j}^2$	From $\int_{\mathrm{BZ}}[T(\partial\tau/\partial k)]^2$
Fe	302 ± 2	279 ± 2	262 ± 3
Ni	747 ± 4	768 ± 6	781 ± 7
Py	521 ± 1	563 ± 2	512 ± 5

were estimated by considering the $\boldsymbol{k}$-mesh convergence (for all three cases) and, additionally, considering the ambiguity of finding the right fits for $\epsilon(\boldsymbol{q})$ in case of analysis of the spin-wave energy dispersion (see Tables V–VII) and of extrapolating $D(\eta)$ to $D(\eta \to 0)$ in case of the $\sum J_{0j} R_{0j}^2$ summation in real space (see Tables VIII–X). A minor contribution to the errors comes also from the $\theta \to 0$ limit when determining $\epsilon(\boldsymbol{q})$ and from having a finite $R_{\max}$ when determining $D(\eta)$. These last two contributions are quite small in comparison with the errors due to the ambiguity of the fitting and/or extrapolating procedure.

Small but distinct differences are evident in Table XI, even though all the approaches use very similar physical assumptions. In particular, in all cases it is assumed that the magnetization direction can be described by vectors $\hat{\boldsymbol{e}}_i$ pinned to atomic sites i [3,4]. All calculations have been performed within the same KKR Green's function formalism, using the SPRKKR code, ensuring that the quantities used in different approaches (coupling constants, spin-wave energies) are consistent.

To point out the differences in the approaches used here, we start by noting that the scalar relativistic spin spiral calculations are performed selfconsistently for each wave vector $\boldsymbol{q}$. As a consequence, the exchange splitting of the energy bands as well as the local magnetic moments are $\boldsymbol{q}$ dependent. Moreover, the spin-spiral energy has been evaluated based on the total energy of the system. The other two approaches, i.e., the methods based on the real-space summation $\sum J_{0j} R_{0j}^2$ according to Eqs. (8)–(10) and on the reciprocal space integral $\int_{\mathrm{BZ}}[T(\partial\tau/\partial k)]^2$ according to Eq. (11), rely on the magnetic force theorem and assume that the magnitude of the magnetic moments does not change if they are tilted (rigid spin approximation). These two approaches are formally equivalent, as was shown, e.g., by Liechtenstein *et al.* [3]. However, small differences in the results occur because the approaches lay different requirements concerning the accuracy of numerical calculations. The requirements laid by the real-space approach are discussed above in detail. The approach based on the BZ integration is very sensitive to the features of the electronic structure because of the $\boldsymbol{k}$ derivatives of the τ matrix in Eq. (11), in contrast to the real-space approach. As a result, a very dense $\boldsymbol{k}$ mesh is needed for the BZ integration to achieve convergence with respect to the number of $\boldsymbol{k}$ points.

The effect of using the magnetic force theorem can be seen from the data in Tables II–IV: It may result in errors of a few percent. The assumption that the magnetic moments do not change their magnitude if they are tilted is plausible for

TABLE XII. Experimental results for spin-wave stiffness D (in meV Å^2) for Fe, Ni, and $Fe_{1-x}Ni_x$ alloy. Each study is identified by a reference and the publication year. The concentration of Ni in $Fe_{1-x}Ni_x$ is given in the last column.

Work		Fe	Ni	$Fe_{1-x}Ni_x$	x
[25]	(1964)	325	400	400	80
[26]	(1966)	350			
[27]	(1968)	314	470		
[28]	(1973)		555		
[29]	(1973)	311			
[30]	(1975)		525	335	68
[31]	(1975)		555		
[32]	(1976)		390		
[33]	(1977)		398		
[34]	(1981)		593		
[35]	(1982)	270	413		
[36]	(1983)		530	390	80
[37]	(1984)	307			
[38]	(1985)		398		
[39]	(2017)			440	80

the systems we are dealing with (see, e.g., Ref. [9] or lower panels of Figs. 1 and 2); nevertheless, small differences still may occur because of this.

As a whole, the differences between the values of D obtained for identical systems by different methods seem to be larger than what could be ascribed to numerical noise. A closer look at Tables V–VII in Sec. III A and Tables VIII–X in Sec. III B reveals that use of just a bit different fitting and extrapolation method can give rise to differences of 5–10%. Even though we put a lot of effort to compensate for ambiguities, some issues probably remained. The third approach does not require any fitting or extrapolation but it requires a very dense $\boldsymbol{k}$ mesh to get truly converged results for the spin-wave stiffness, making the calculations very demanding. We assume that the results obtained by means of Eq. (11) could still be improved upon by increasing the $\boldsymbol{k}$-mesh density but only at very high (impractical) computational costs.

On the other hand, possible errors of the procedures to calculate D concern mostly the absolute values, not the trends. For example, application of the real-space summation Eqs. (8)–(10) to Py doped with V, Gd, and Pt led to a good theoretical description of the way the dopants influence the spin-wave stiffness, in agreement with experiment [20]. Likewise, the dependence of the spin-wave stiffness of the $Fe_{1-x}Ni_x$ alloy on its composition can be properly described both by fitting the spin-wave energy dispersion according to Eqs. (3) and (7) and by direct evaluation of D via a reciprocal-space integral according to Eq. (11) [14].

Uncertainty in determining the theoretical values of the stiffness constants D for Fe, Ni, and Py is accompanied by uncertainty in experiment. We summarize in Table XII a selection of available experimental data; a more complete list can be found, e.g., in Tables 7 and 8 of Vaz *et al.* [1]. One can see that the spread of results of different studies is quite large—about 15% for Fe and Py and about 20% for Ni. A critical assessment of experimental studies is beyond our scope. Despite the relatively large spread of the data, Tables XI–XII indicate that our theory agrees well with experiment for Fe,

whereas for Ni and Py the agreement is less good. Tentatively, this is linked to problems with describing the exchange coupling of Ni in terms of the coupling constants [40,41]. Some errors could be also introduced because of the restrictions of our computational scheme, notably the ASA; nevertheless, full-potential effects are usually small in close-packed metals such as those we are dealing with. It is more likely that the assumption of rigid moments is not fully justified for Ni and its alloys.

Even though our study has been performed for Fe, Ni, and Py, it is focused on analyzing and discussing concepts that have to be dealt with when studying the spin-wave stiffness for any material. Metallic systems such as those we investigate here represent the most difficult case as concerns evaluating the stiffness by means of a weighted sum of the coupling constants (Sec. III B). This is because, for metals, the coupling constants J_{ij} decay with distance as $1/R_{ij}^3$ [5], i.e., relatively slowly. For semiconductors and insulators, the opening of a gap leads to an exponential decay of the exchange coupling, as $1/R_{ij}^3 \exp(-R_{ij}/\lambda)$ [5,42], improving the convergence of the expression Eq. (5) considerably. This will enable us to employ larger R_{max} and lower η, possibly disposing of the damping term $\exp(-\eta R_{0j}/R_{01})$ altogether. Increasing the disorder (as, for example, in the case of high-entropy alloys) will introduce an exponential spatial damping of the exchange coupling as well [42].

The analyses performed in Sec. III enable us to draw some recommendations how to evaluate the stiffness constant D. In general, evaluating D by means of fitting $\epsilon(\boldsymbol{q})$ by a polynomial is less demanding and more reliable than evaluating D by means of extrapolating $D(\eta)$ obtained by means of $J_{0j}R_{0j}^2$ summation. The convergence with the $\boldsymbol{k}$-mesh density is better in the former case and, moreover, extrapolation required in the latter case is always an ambiguous procedure. However, fitting $\epsilon(\boldsymbol{q})$ by a polynomial to determine the coefficient at the quadratic term is not without risks either. Higher powers should be included in the fitting polynomial Eq. (17); employing just a simple quadratic fit as done, e.g., in Ref. [43] may not always be sufficient.

In many cases, calculating the energy dispersion $\epsilon(\boldsymbol{q})$ is difficult or impractical (e.g., for multicomponent systems with substitutional disorder). Extrapolating $D(\eta)$ down to $\eta \to 0$ then remains the only viable option. In such cases, extra care has to be taken and the robustness of the selected extrapolation procedure should be checked. For example, application of a quadratic extrapolation within the $\eta \in [0.6, 1.0]$ interval (employed, e.g., for transition metals [5] or for Heusler alloys [18]) to the systems investigated here would lead to a systematic undershooting of D by about 10%. Of course, these conditions have to be explored specifically for each system considered. Evaluating D directly in reciprocal space Eq. (11) does not suffer from the pitfalls of fitting or extrapolating but it is numerically demanding and sensitive to the details of the electronic structure.

V. CONCLUSIONS

Evaluating the spin-wave stiffness constant D by current schemes is technically difficult and potentially numerically unstable. Differences between values obtained by different

methods of 5–10% remain even if care is taken to make all the calculations consistent with each other and well converged. The agreement between theoretical values and experimental data is good in case of Fe but significant differences occur for Ni and permalloy $Fe_{0.19}Ni_{0.81}$.

Calculating the stiffness constant D usually involves either fitting the long-wavelength part of the spin-wave energy dispersion $\epsilon(\boldsymbol{q})$ by a polynomial, or extrapolating the values $D(\eta)$ obtained via a real-space summation of weighted exchange coupling constants to zero damping, $\eta \to 0$. Both procedures are tricky and quite sensitive to technical details how the fitting or extrapolation is done.

[1] C. A. F. Vaz, J. A. C. Bland, and G. Lauhoff, Rep. Prog. Phys. **71**, 056501 (2008).

[2] J. Kübler, *Theory of Itinerant Electron Magnetism*, International Series of Monographs on Physics (Oxford University Press, Oxford, 2000).

[3] A. I. Liechtenstein, M. I. Katsnelson, and V. A. Gubanov, J. Phys. F: Met. Phys. **14**, L125 (1984).

[4] A. I. Liechtenstein, M. I. Katsnelson, V. P. Antropov, and V. A. Gubanov, J. Magn. Magn. Mater. **67**, 65 (1987).

[5] M. Pajda, J. Kudrnovský, I. Turek, V. Drchal, and P. Bruno, Phys. Rev. B **64**, 174402 (2001).

[6] P. Yu, X. F. Jin, J. Kudrnovský, D. S. Wang, and P. Bruno, Phys. Rev. B **77**, 054431 (2008).

[7] F. Pan, J. Chico, A. Delin, A. Bergman, and L. Bergqvist, Phys. Rev. B **95**, 184432 (2017).

[8] O. N. Mryasov, A. J. Freeman, and A. I. Liechtenstein, J. Appl. Phys. **79**, 4805 (1996).

[9] N. M. Rosengaard and B. Johansson, Phys. Rev. B **55**, 14975 (1997).

[10] R. H. Brown, D. M. C. Nicholson, X. Wang, and T. C. Schulthess, J. Appl. Phys. **85**, 4830 (1999).

[11] M. van Schilfgaarde and V. P. Antropov, J. Appl. Phys. **85**, 4827 (1999).

[12] S. Morán, C. Ederer, and M. Fähnle, Phys. Rev. B **67**, 012407 (2003).

[13] S. Shallcross, A. E. Kissavos, V. Meded, and A. V. Ruban, Phys. Rev. B **72**, 104437 (2005).

[14] S. Mankovsky, S. Polesya, and H. Ebert, Phys. Rev. B **99**, 104427 (2019).

[15] H. Ebert, D. Ködderitzsch, and J. Minár, Rep. Prog. Phys. **74**, 096501 (2011).

[16] H. Ebert, *The SPRKKR package, version 7*, http://olymp.cup.uni-muenchen.de/ak/ebert/SPRKKR (2014).

[17] S. Mankovsky, G. H. Fecher, and H. Ebert, Phys. Rev. B **83**, 144401 (2011).

[18] J. Thoene, S. Chadov, G. Fecher, C. Felser, and J. Kübler, J. Phys. D: Appl. Phys. **42**, 084013 (2009).

[19] P. Dürrenfeld, F. Gerhard, J. Chico, R. K. Dumas, M. Ranjbar, A. Bergman, L. Bergqvist, A. Delin, C. Gould, L. W. Molenkamp, and J. Åkerman, Phys. Rev. B **92**, 214424 (2015).

[20] O. Šipr, S. Mankovsky, and H. Ebert, Phys. Rev. B **100**, 024435 (2019).

[21] H. Ebert, H. Freyer, A. Vernes, and G.-Y. Guo, Phys. Rev. B **53**, 7721 (1996).

[22] O. Šipr, S. Bornemann, H. Ebert, and J. Minár, J. Phys.: Condens. Matter **26**, 196002 (2014).

[23] O. Šipr, S. Mankovsky, S. Polesya, S. Bornemann, J. Minár, and H. Ebert, Phys. Rev. B **93**, 174409 (2016).

[24] K. Terakura, N. Hamada, T. Oguchi, and T. Asada, J. Phys. F: Met. Phys. **12**, 1661 (1982).

[25] M. Hatherly, K. Hirakawa, R. D. Lowde, J. F. Mallett, M. W. Stringfellow, and B. H. Torrie, Proc. Phys. Soc. London **84**, 55 (1964).

[26] T. G. Phillips, Proc. R. Soc. London A **292**, 224 (1966).

[27] M. W. Stringfellow, J. Phys. C: Solid State Phys. **1**, 950 (1968).

[28] H. A. Mook, J. W. Lynn, and R. M. Nicklow, Phys. Rev. Lett. **30**, 556 (1973).

[29] P. C. Riedi, Phys. Rev. B **8**, 5243 (1973).

[30] M. Hennion, B. Hennion, A. Castets, and D. Tocchetti, Solid State Commun. **17**, 899 (1975).

[31] A. T. Aldred, Phys. Rev. B **11**, 2597 (1975).

[32] T. Maeda, H. Yamauchi, and H. Watanabe, J. Phys. Soc. Jpn. **40**, 1559 (1976).

[33] P. Riedi, Physica B+C **91**, 43 (1977).

[34] J. W. Lynn and H. A. Mook, Phys. Rev. B **23**, 198 (1981).

[35] R. Pauthenet, J. Appl. Phys. **53**, 2029 (1982).

[36] I. Nakai, J. Phys. Soc. Jpn. **52**, 1781 (1983).

[37] C. Loong, J. M. Carpenter, J. W. Lynn, R. A. Robinson, and H. A. Mook, J. Appl. Phys. **55**, 1895 (1984).

[38] P. W. Mitchell and D. M. Paul, Phys. Rev. B **32**, 3272 (1985).

[39] Y. Yin, M. Ahlberg, P. Dürrenfeld, Y. Zhai, R. K. Dumas, and J. Åkerman, IEEE Magn. Lett. **8**, 1 (2017).

[40] P. Bruno, Phys. Rev. Lett. **90**, 087205 (2003).

[41] J. Kudrnovský, V. Drchal, and P. Bruno, Phys. Rev. B **77**, 224422 (2008).

[42] J. Kudrnovský, I. Turek, V. Drchal, F. Máca, P. Weinberger, and P. Bruno, Phys. Rev. B **69**, 115208 (2004).

[43] F. J. dos Santos, M. dos Santos Dias, and S. Lounis, Phys. Rev. B **95**, 134408 (2017).